Journal of Materials Chemistry A

ROYAL SOCIETY OF CHEMISTRY

PAPER

View Article Online
View Journal | View Issue

Cite this: J. Mater. Chem. A, 2025, 13, 30151

Design of phthalocyanine metal complexes for efficient far-red to near-IR light-initiated photopolymerizations

Connor J. O'Dea,[a] Lauren M. Loftus,[bc] Tod A. Grusenmeyer,[b] Jussi Isokuortti,[a] Justin Ong,[a] Sean T. Roberts *[a] and Zachariah A. Page *[ad]

Received 16th July 2025
Accepted 11th August 2025

DOI: 10.1039/d5ta05756f

rsc.li/materials-a

Efficient near-infrared (NIR) photopolymerization is promising for applications such as hydrogel bioprinting, composite manufacturing, and other technologies that benefit from deep light penetration and low-energy activation. Yet, design principles for optimizing NIR photoinitiators, particularly those based on earth-abundant or metal-free elements, remain limited. Here, a library of phthalocyanine (**Pc**) and naphthalocyanine (**Nc**) derivatives was synthesized, characterized, and evaluated as photoredox catalysts for NIR-induced radical polymerizations. Variations in metal center (Zn, Si, Pd), α-substitution (pentyl or butoxy), and π-extension (**Pc** *vs.* **Nc**) enabled tuning of light absorption, excited-state energies and lifetimes, and triplet excited state quantum yields. Polymerization kinetics were quantified using real-time FTIR spectroscopy under LED irradiation (740–940 nm), with photon absorption normalized to allow direct comparison of internal quantum yields. This work provides a framework for quantitative benchmarking of NIR photoinitiators under controlled conditions. Among the catalysts studied, a Pd–**Pc** complex showed the highest internal efficiency, while a Si–**Nc** catalyst outperformed a leading commercial cyanine initiator, highlighting the potential of silicon as a sustainable alternative to precious metals. These results establish clear structure–property relationships and offer guiding principles for the design of next-generation NIR photoinitiators suited for biomedical and advanced manufacturing technologies.

Zachariah A. Page

Zachariah A. Page is an Associate Professor at The University of Texas at Austin, where his group develops light-driven methods to create and manipulate plastics. He earned a B. S. in Chemistry from Juniata College and a PhD in Polymer Science and Engineering from the University of Massachusetts Amherst with Todd Emrick. He then completed postdoctoral training with Craig Hawker at UC Santa Barbara. Since joining UT Austin in 2018, he has advanced photopolymerization chemistries and pioneered visible light 3D printing, publishing 90+ papers and 20+ patents. His honors include PECASE, Sloan, NSF CAREER, AFOSR YIP, Camille Dreyfus, and Cottrell Scholar awards.

Introduction

Phthalocyanine (**Pc**), naphthalocyanine (**Nc**), and their metalated analogs are macrocyclic compounds structurally related to naturally occurring porphyrins. These electron-rich, aromatic molecules – featuring a conjugated 18π core electron system with pyrrolic units fused to benzene rings – have long attracted attention due to their exceptional thermal and chemical stability. Discovered serendipitously during the industrial synthesis of phthalimide, iron **Pc** initially drew interest as a pigment,[1] prompting decades of research into metal complexes[2] and π-extended species.[3] This prolific development led to applications in areas such as photovoltaics,[4,5] chemical sensors,[6,7] non-linear optics,[8] liquid crystals,[9,10] and photodynamic therapy, supported by the formation of the International Society of Porphyrins and Phthalocyanines in 2000.[11]

More recently, **Pcs** and **Ncs** have emerged as promising candidates for photoredox catalysis, including (controlled) radical polymerizations.[12–14] Their strong visible and near-

[a]Department of Chemistry, The University of Texas at Austin, Austin, Texas 78712, USA. E-mail: zpage@cm.utexas.edu; roberts@cm.utexas.edu
[b]Materials and Manufacturing Directorate, Air Force Research Laboratory, Wright-Patterson Air Force Base, OH 45433, USA
[c]Azimuth Corporation, A Core4ce LLC Company, 2970 Presidential Dr #200, Fairborn, OH 45342, USA
[d]McKetta Department of Chemical Engineering, The University of Texas at Austin, Austin, Texas 78712, USA

infrared (NIR) absorption, high extinction coefficients, and synthetic tunability make them attractive scaffolds for photocatalyst design. However, despite these favorable properties, their use in low-energy (long-wavelength) photopolymerization remains limited. The absence of systematic structure–reactivity studies has hindered the development of design rules for maximizing photopolymerization efficiency across different metal centers, substituents, and dye architectures.

This gap is particularly significant given the growing demand for photopolymerizations that operate under long-wavelength light. Such conditions improve light penetration through UV-opaque or scattering media – such as biological tissues and nanocomposite materials – due to the inverse fourth-power dependence of Rayleigh scattering on wavelength.[15] As a result, efficient far-red to NIR photoinitiators are needed to advance emergent photocurable technologies, such as additive manufacturing. Many such systems rely on triplet sensitization to enable bimolecular electron transfer, as the longer lifetimes of triplet excited states relative to singlets increase the probability of productive redox events per photon absorbed. However, most known triplet sensitizers depend on precious metals (*e.g.*, Pd, Ir), raising sustainability concerns and motivating the development of alternatives based on earth-abundant elements like Zn and Si.

In this study, we address these challenges through the synthesis and evaluation of a library of **Pc** and **Nc** derivatives featuring varied metal centers, non-peripheral substituents, and π-extension. Using a normalized photon absorption approach, we systematically compare their photophysical properties and catalytic performance in NIR-induced radical polymerizations. These results establish critical structure–property relationships and define new design principles for sustainable, high-efficiency NIR photocatalysts.

Results and discussion

Material scope & optical characterization

A series of metalated **Pc** and **Nc** derivatives were selected based on precedent for efficient singlet oxygen sensitization *via* triplet energy transfer.[16–18] Given the longer lifetimes of triplet (∼μs) *versus* singlet (∼ns) excited states, and our prior findings, extended triplet lifetimes were expected to enhance bimolecular electron transfer and enable Type II photoinitiation.[19,20] Building on this premise, three macrocyclic scaffolds were synthesized (Scheme S1) covering peak absorption values from the far-red (∼700–780 nm) into the near-infrared (NIR, ∼780–870 nm), enabling a systematic evaluation of how absorption wavelength impacts photocatalytic performance. Bathochromic

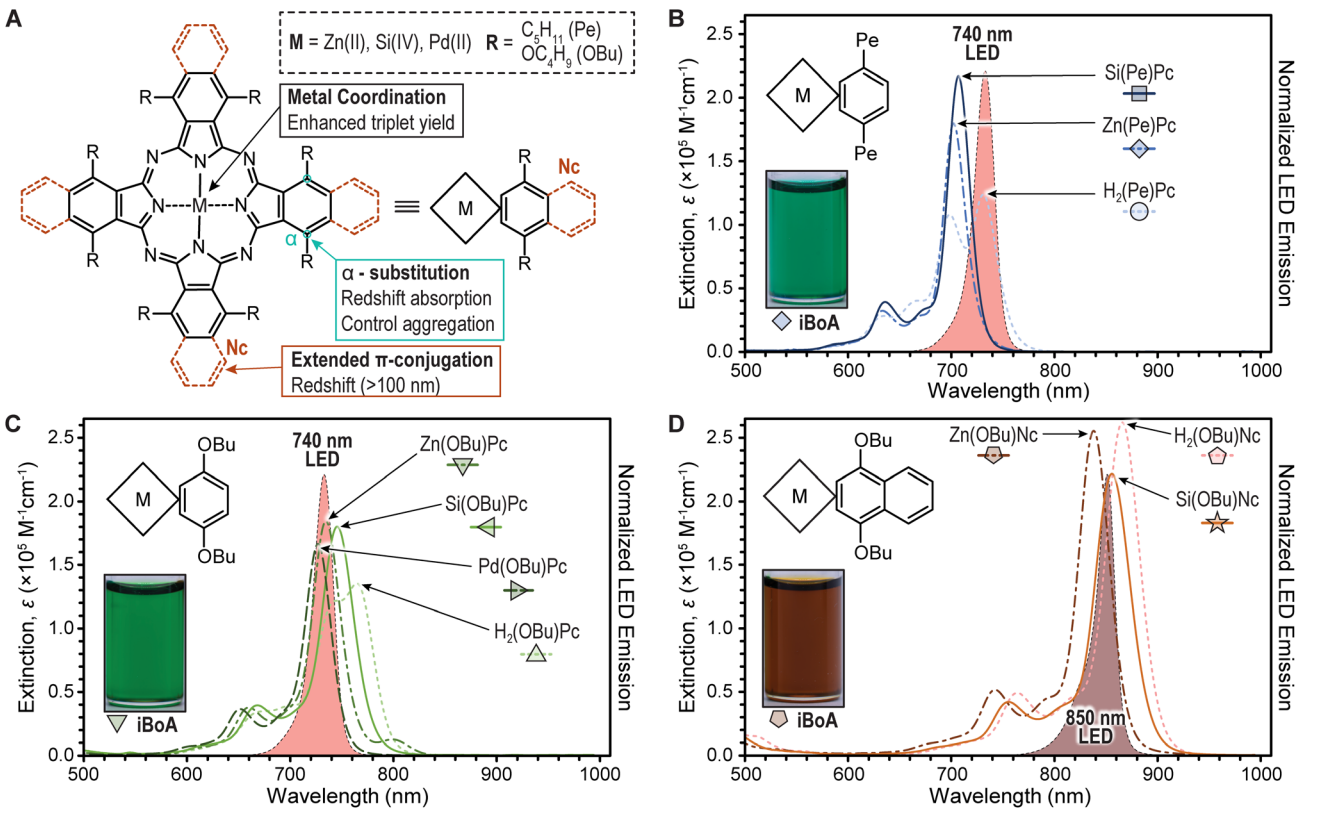

Fig. 1 Molecular structures and optical properties of phthalocyanine (**Pc**) and naphthalocyanine (**Nc**) derivatives investigated in this study. (A) General molecular structure highlighting positions of metal coordination (*M*), α-substitution (*R*), and benzoannulation (**Nc** *vs.* **Pc**), with corresponding shorthand notation. (B–D) UV-vis absorption spectra (solid lines) of each photosensitizer in **iBoA** overlaid with normalized LED emission profiles (shaded curves) used for photopolymerization at 740, 780, 850, and 940 nm. (B) Pentyl-substituted **Pc** derivatives; (C) *n*-butoxy-substituted **Pc** derivatives; (D) *n*-butoxy-substituted **Nc** derivatives. Inset photographs show representative **Pc** and **Nc** solutions in **iBoA** (0.48 mM).

shifts in absorption were achieved through: (1) extension of π-conjugation *via* benzoannulation (**Pc** to **Nc**), which narrows the $S_0 \rightarrow S_1$ energy gap;[21–23] (2) introduction of electron-donating alkoxy groups at the α-position to destabilize the HOMO energy, which raises the ground-state energy (S_0);[24,25] and (3) coordination of electron-deficient metals to stabilize the LUMO energy, which lowers the first excited singlet state energy (S_1).[26,27] In addition to shifting absorption to longer wavelengths, α-substitution improved solubility, while metalation was employed to enhance intersystem crossing and triplet yield.

Metal complexes of Zn, Si, and Pd were prepared from the corresponding free-base **Pc** and **Nc** derivatives (Fig. 1A). Additionally, Al metal complexes were initially prepared but found to be unstable under the reaction conditions, and were therefore excluded from the main text (see SI for details). In contrast to unsubstituted **ZnPc**, which shows poor solubility in organic solvents and absorbs maximally at ~675 nm, our functionalized derivatives – **Zn(Pe)Pc**, **Zn(OBu)Pc**, and **Zn(OBu)Nc** – exhibited excellent solubility in toluene and λ_{max} values of 706, 739, and 848 nm, respectively (Fig. 1B–D). Extinction coefficients were measured using the Beer–Lambert Law in both dilute solution (~μM) and in concentrated thin films (~mM) formulated in isobornyl acrylate (**iBoA**), the monomer used in subsequent photopolymerization studies. Under both conditions, **Pc** derivatives showed strong absorptivity, with peak molar extinction coefficients of ~140 000–220 000 M^{-1} cm^{-1} in the 700–740 nm range. **Nc** derivatives exhibited even higher values of ~220 000–340 000 M^{-1} cm^{-1} near 850 nm (Fig. S1–S11). Due to poor solubility in the monomer, **iBoA**, **Pd(Pe)Pc** and **Pd(OBu)Nc** were excluded from further study. Overall, the strong absorptivity of these metalated **Pc** and **Nc** dyes across the far-red and NIR spectrum suggested excellent compatibility with 740, 780, 850, and 940 nm LED light sources for low-energy photopolymerizations (Fig. S12).

Photopolymerization

Building on the strong absorptivity of the **Pc** and **Nc** derivatives across the far-red to NIR range, we evaluated their performance as photoredox catalysts (PRCs) in a model three-component Type II photoinitiation system in **iBoA**. This formulation included a donor co-initiator, 2-(butyryloxy)-*N*,*N*,*N*-trimethylethan-1-aminium butyltriphenylborate (Borate V, 2.4 mM), an acceptor co-initiator, 4-(octyloxy)phenyliodonium hexafluoroantimonate (H-Nu 254, 24 mM), and a **Pc** or **Nc** derivative as the PRC (2.4 mM). The monomer, **iBoA**, was selected for its biobased origin, low volatility, and ability to solubilize the photosystem (Fig. S13). Photopolymerization kinetics were monitored *in situ* using real-time Fourier transform infrared (RT-FTIR) spectroscopy in attenuated total reflectance (ATR) mode (Fig. 2 and S14). Monomer-to-polymer conversion (ρ) was quantified by integrating the vinylic C=C–H bending between 770–830 cm^{-1} (Fig. S15). Conversion of **iBoA** typically plateaued around 80%, consistent with vitrification due to the high glass transition temperature of the resulting homopolymer (T_g = 94 °C).[28] To eliminate oxygen inhibition, samples were degassed with argon for 10 minutes

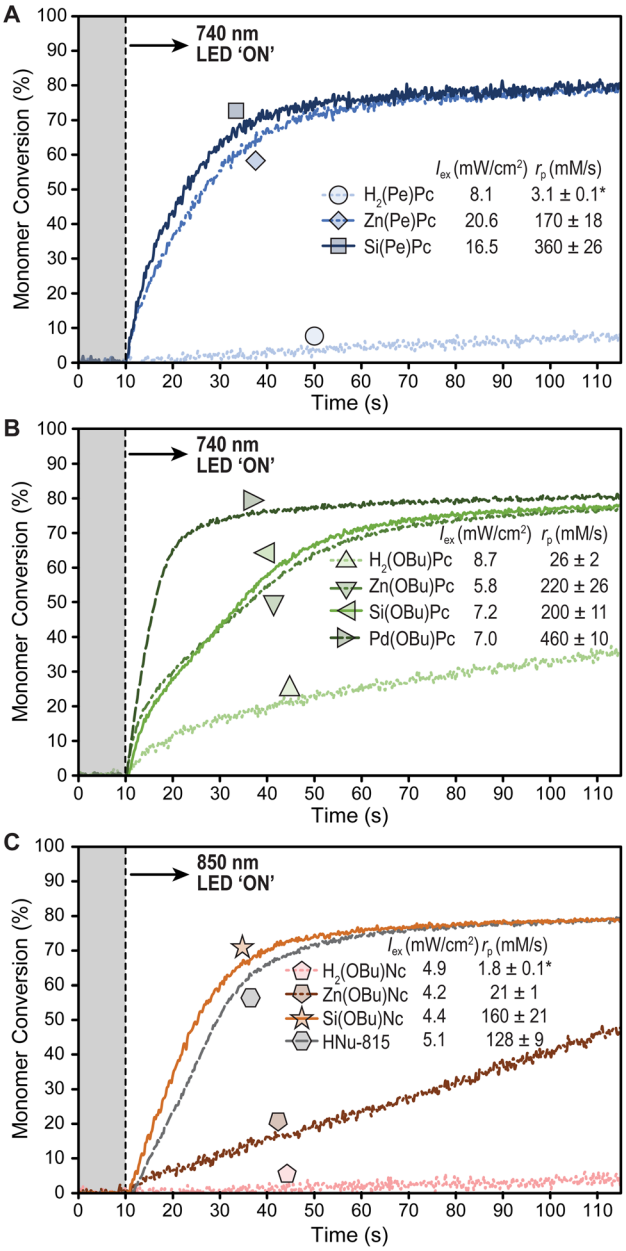

Fig. 2 Real-time photopolymerization kinetics for **Pc** and **Nc** derivatives monitored by RT-FTIR under LED irradiation. (A) Pentyl-substituted phthalocyanine (PePc) derivatives activated by a 740 nm LED. (B) Butoxy-substituted phthalocyanine (OBuPc) derivatives under a 740 nm LED. (C) Butoxy-substituted naphthalocyanine (OBuNc) derivatives under an 850 nm LED, compared with commercial cyanine-based photocatalyst, **HNu-815**. LED activation occurred at t = 10 s (indicated by vertical dashed line and "LED ON"). Irradiation intensities (I_0) were adjusted to equalize the initial photon absorption rate across all photocatalysts. Monomer conversion (%) was monitored as a function of time, with initial polymerization rates ($r_{p,20\%}$) extracted from the linear region up to 20% conversion. *Rate calculated from slope between 40 and 120 s.

and run under continuous argon flow within a glass chamber during irradiation. To facilitate comparisons across **Pc** and **Nc** derivatives, the initial photon absorption rate for each system was calculated by integrating the spectral overlap between the dye's molar extinction coefficient and the emission spectrum of

the selected LED (Fig. 1B–D). From this data, irradiation intensities were adjusted to normalize the photon absorption rate across all conditions (1×10^{15} photons cm^{-2} s^{-1}), enabling direct quantification of photopolymerization quantum yields.

Photopolymerization studies began with the **Pc** derivatives using far-red (740 nm) LED irradiation at intensities ranging from 7.0 to 20.6 mW cm^{-2}. Irradiation was initiated 10 seconds into each run to confirm temporal control (Fig. 2A, B, S16–S22 and Table S1). The initial polymerization rate (r_p) was calculated up to 20% monomer conversion (ρ), where the kinetics remained linear (see SI Section S2.3 for details). In all cases, metalation significantly enhanced $r_{p,20\%}$ compared to the corresponding free-base Pc derivatives. This enhancement was especially pronounced in the pentyl-substituted series (Fig. 2A). The free-base compound **H_2(Pe)Pc** exhibited very slow conversion, failing to reach 20% within 2 minutes of irradiation and yielding $r_p = 3.1 \pm 0.1$ mM s^{-1}. In contrast, metalated analogs **Zn(Pe)Pc** and **Si(Pe)Pc** achieved dramatically higher rates of 170 ± 18 mM s^{-1} and 360 ± 26 mM s^{-1}, respectively – over 50-fold higher than **H_2(Pe)Pc**.

In the butoxy-substituted **Pc** series (Fig. 2B), despite receiving the highest LED intensity (8.7 mW cm^{-2}) to normalize photon absorption, the free-base derivative **H_2(OBu)Pc** again displayed the lowest activity ($r_{p,20\%} = 26 \pm 2$ mM s^{-1}). Metalation with Zn, Si, and Pd led to significantly faster rates of 220 ± 26, 200 ± 11, and 460 ± 10 mM s^{-1}, respectively. Interestingly, both Zn and Si derivatives showed a noticeable decline in polymerization rate beyond the initial period, hypothesized to result from photocatalyst degradation, as evidenced by visible color change. This was subsequently investigated using *in situ* UV-vis absorption (see photodegradation section).

The **Nc** derivatives were next evaluated using an 850 nm NIR LED (Fig. 2C, S23–S26 and Table S1). Here, the Si derivative **Si(OBu)Nc** exhibited a markedly faster polymerization rate ($r_{p,20\%} = 160 \pm 21$ mM s^{-1}) than its Zn analog **Zn(OBu)Nc** (21 ± 1 mM s^{-1}) under a low intensity irradiation of 4.4 mW cm^{-2} – an approximately 8-fold increase. To benchmark performance, **Si(OBu)Nc** was directly compared to a leading commercial NIR photoinitiator, **HNu-815**, under equivalent photon absorption conditions using the calculated intensities (4.4 and 5.1 mW cm^2, respectively). Since **HNu-815** comprises a cationic cyanine dye paired with Borate V as the counteranion, only **HNu-254** (24 mM) was added to **iBoA** formulations to ensure equimolar co-initiator concentrations. Under these matched conditions, **Si(OBu)Nc** consistently outperformed **HNu-815**, with an average $r_{p,20\%}$ of 128 ± 9 mM s^{-1}, approximately 1.2× higher than the commercial benchmark. The high extinction coefficient and red-shifted absorption of **Si(OBu)Nc** relative to the commercial photoinitiator facilitated photopolymerizations with a 940 nm LED using an equivalent photon absorption rate (Fig. S27–S28) These results indicate that **Si(OBu)Nc** exhibits a modest increase in internal quantum efficiency relative to the cyanine-based standard (discussed further below).

Energy landscape & quantum yield

To elucidate the origin of differences in photopolymerization efficiency, we characterized the excited-state energetics and dynamics of the photocatalysts and quantified their corresponding polymerization quantum yields. Excited-state energy levels were determined using a combination of cyclic voltammetry, optical absorption and emission spectroscopy (Fig. 3A, S29–S31 and Table S2). Singlet excited state energies (E_{S1}) were determined from fluorescence emission maxima (Fig. S32–S43), which followed a similar trend to that observed for the HOMO–LUMO energy gap (ΔE) from cyclic voltammetry, following the order Pd > Si ≥ Zn for the metalated derivatives (Table S2). Triplet excited-state energies (E_{T1}) were estimated from phosphorescence emission at 77 K, with literature values substituted for **Si(OBu)Pc** and **Si(OBu)Nc** due to their weak emissivity.[29,30] Among the catalysts, Pd-containing derivatives consistently exhibited the highest triplet energies, favoring electron transfer to the acceptor co-initiator. Singlet oxygen phosphorescence at

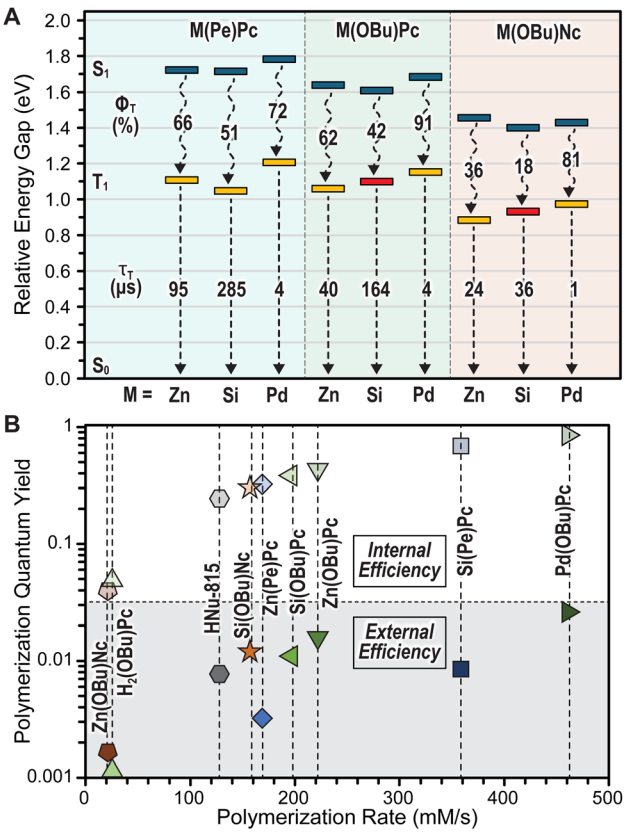

Fig. 3 Excited-state energy landscape and photopolymerization efficiency of Pc and Nc derivatives. (A) Energy diagram illustrating the excited-state properties relative to the ground state (S_0, baseline) for each metalated dye. Singlet excited-state energies (S_1, blue bars) were calculated from the fluorescence emission maximum in toluene. Triplet excited-state energies (T_1, yellow bars) were estimated from phosphorescence spectra, with values for Si(OBu)Pc and Si(OBu)Nc (red bars) taken from literature due to weak emission. The dashed wavy line represents the triplet quantum yield (Φ_T). Dashed straight lines indicate triplet lifetimes (τ_T), from nanosecond transient absorption spectroscopy. (B) Polymerization quantum yield plotted as a function of photopolymerization rate. External efficiency (bottom, dark symbols) was calculated as the polymerization rate ($r_{p,20\%}$) normalized by incident photon flux; internal efficiency (top, light symbols) was determined by normalizing to the actual photon absorption rate.

1270 nm was used as a proxy for triplet quantum yield (Φ_T) for the **Pc** series (Fig. S44–S45), whereas photosensitization with TIPS-pentacene was used with the **Nc** series for triplet energy matching (Fig. S46–S49 and Table S3). The triplet quantum yield followed the trend of Pd > Zn > Si and except for **Si(OBu)Nc**, all derivatives exhibited appreciable Φ_T values exceeding ~35% (Table S4). Notably, Pd derivatives showed the highest Φ_T values (70–90%) and correspondingly the highest $r_{p,20\%}$, indicating a strong correlation between triplet yield and photopolymerization performance.

While these findings highlight the importance of triplet yield, transient absorption spectroscopy revealed an important trade-off. Pd derivatives, despite their high Φ_T and E_{T1}, exhibited triplet lifetimes (τ_t) at least 10-fold shorter than Zn analogs, which in turn were ~1.5–4× shorter than those of Si derivatives (Fig. S50–S61). These extended triplet lifetimes, especially in the Si-based photocatalysts, are expected to enhance the probability of bimolecular redox events, particularly at lower photocatalyst concentrations. Together, these results suggest that triplet yield, energy, and lifetime contribute distinctly to overall photocatalytic performance: while high triplet yield and energy favor rapid initiation, long triplet lifetimes support radical generation under diffusion-limited conditions.

To quantify overall photopolymerization efficiency, we calculated both external and internal quantum yields. External efficiency was defined as the polymerization rate (mM s^{-1}) normalized by the incident photon flux, while internal efficiency accounted for the actual photon absorption rate (Fig. 3B and Table S5; see SI Section S2.5 for details). Thus, a quantum yield of one implies that each absorbed photon results in the consumption of one monomer molecule. However, since each initiating radical leads to chain-growth polymerization, this can exceed unity. A future refinement would be to assess the number of initiating radicals generated per absorbed photon to decouple initiation from propagation events. Despite this complexity, the relative quantum yields under standardized conditions provided a meaningful comparison across the series. **Pd(OBu)Pc** exhibited the highest external and internal quantum yields, reinforcing the role of high triplet yield and energy in driving efficient polymerization. Interestingly, the next-highest internal quantum yield was observed for **Si(Pe)Pc**, which was nearly two-fold greater than the remaining Si and Zn derivatives and 2.8-fold higher than the commercial benchmark, **HNu-815**. The strong performance seen for **Pd(OBu)Pc** suggests that under the current conditions, enhancing triplet yield and/or energy has a greater impact on efficiency than triplet lifetime alone, although, each are important for optimizing photoinitiator design.

Photodegradation

To investigate the origin of photocatalyst degradation – visibly observed as a color change during irradiation – we monitored the optical stability of thin films (20 μm) for the butoxy-substituted **Pc** series using *in situ* optical absorption spectroscopy (Fig. 4A, S62–S66 and Table S6). Catalyst concentration was estimated from the average absorbance during a 10-second dark period using the Beer–Lambert law and then tracked during two minutes of continuous 740 nm irradiation. All butoxy-**Pc** derivatives exhibited a decrease in Q-band absorbance, indicative of photobleaching, with the most pronounced degradation observed for **Zn(OBu)Pc** (Fig. 4B).

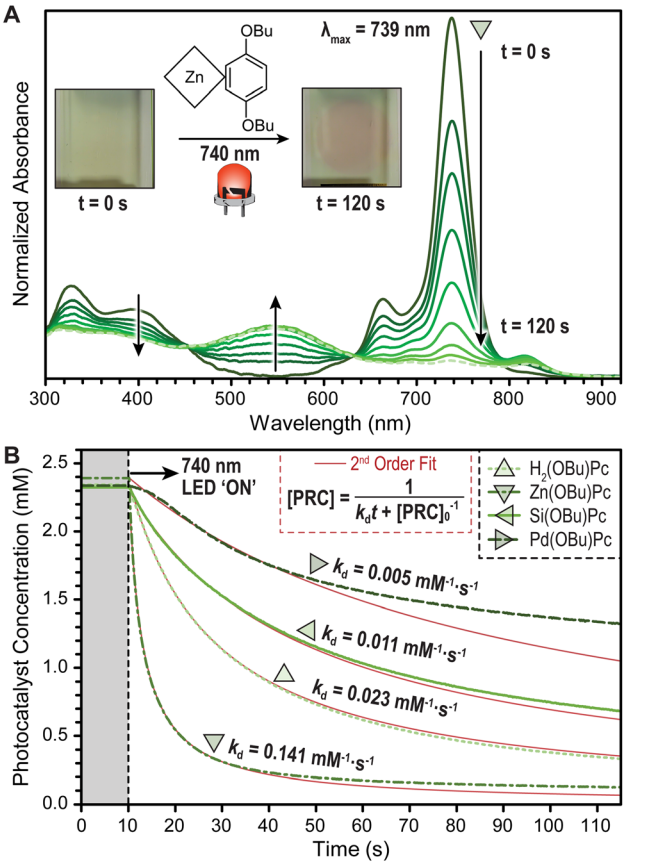

Fig. 4 *In situ* monitoring of photocatalyst degradation during photopolymerization. (A) Optical absorbance spectra of **Zn(OBu)Pc** in the complete **iBoA** resin formulation during continuous 740 nm LED irradiation (photon flux = 1×10^{15} photons cm^{-2} s^{-1}), collected every second over a 2-minute period. Insets: photographs of **Zn(OBu)Pc** resin before and after irradiation, showing visible discoloration. (B) Photoredox catalyst concentration ([PRC]) profiles of butoxy-substituted phthalocyanine derivatives (Zn, Si, Pd, and H_2) during 740 nm irradiation at equal initial absorbed photon rates. Catalyst concentration was calculated from absorbance values in the pre-irradiation region (t < 10 s) and fit to second-order decay kinetics (red lines).

Kinetic analysis of early-time absorbance loss revealed apparent second-order decay behavior. The photodegradation rate constant (k_d) for **Zn(OBu)Pc** was 0.141 mM^{-1} s^{-1}, approximately 13-fold and 28-fold greater than that of **Si(OBu)Pc** (0.011 mM^{-1} s^{-1}) and **Pd(OBu)Pc** (0.005 mM^{-1} s^{-1}), respectively. Notably, the free-base analogue **H_2(OBu)Pc** showed the second-highest k_d (0.023 mM^{-1} s^{-1}), suggesting that metalation – particularly with Pd or Si – improves photostability. Potential mechanisms of degradation include protonation of meso-nitrogen sites by Lewis acids generated from iodonium salt decomposition,[24,31] as well as reactions with carbon-centered radicals and singlet oxygen species, where the latter has been

shown to degrade phthalocyanines into open-chain pyrrolic fragments.[32,33] In cyclic voltammetry, Zn derivatives show a negative shift in the first oxidation potential ($E_{ox,1}$) relative to the free-base, consistent with destabilization of the HOMO energy making them more susceptible toward oxidative degradation (Table S2 and Fig. S29–S31).

To further probe degradation pathways, we conducted systematic component testing with **Zn(OBu)Pc** as the model photocatalyst (Fig. S67–S68 and Table S7). Photopolymerization and photobleaching rates were evaluated in resins containing: (i) **Zn(OBu)Pc** only, (ii) **Zn(OBu)Pc** + **HNu-254**, (iii) Borate V + **HNu-254**, and (iv) the full three-component photosystem. Notably, Borate V was not miscible in **iBoA** on its own, suggesting the formation of a donor–acceptor complex with **HNu-254** that has enhanced solubility. As expected, no polymerization was observed upon 740 nm irradiation in formulations lacking either the **Pc** or both co-initiators. Interestingly, the **Zn(OBu)Pc** + **HNu-254** combination led to slow polymerization kinetics ($r_p = 3.3$ mM s^{-1}) only reaching a maximum conversion of 13% after 2 minutes, but showed a high rate of photodegradation ($k_d = 0.049$ mM^{-1} s^{-1}), indicating that inclusion of an electron donor is crucial for polymerization, and that the electron acceptor leads to considerable catalyst decomposition. While further mechanistic studies are warranted, these results reinforce the importance of a complete three-component Type II photoinitiating system and offer a plausible explanation for the observed decrease in polymerization rate after rapid initial conversion in Zn-based systems.

Conclusions

Phthalocyanine (**Pc**) and naphthalocyanine (**Nc**) derivatives with tunable absorption profiles from the far-red to near-infrared (NIR) region enabled efficient photopolymerization under low-intensity irradiation (<10 mW cm^{-2}). Metalation with Zn, Si, or Pd significantly increased triplet yields and enhanced performance as Type II photoredox catalysts. By normalizing photon absorption across wavelengths, we systematically correlated triplet energy, yield, and lifetime with polymerization efficiency. **Pd(OBu)Pc** exhibited the highest internal quantum yield, while **Si(OBu)Nc** outperformed the commercial NIR initiator **HNu-815**, attributed to its combination of strong absorption and a long-lived triplet state. Importantly, Si-based derivatives demonstrated greater photostability than their Zn analogues and offer a compelling advantage over Pd as an earth-abundant and non-toxic metal. Moreover, the octahedral coordination geometry of Si provides a promising platform for future axial functionalization to tailor solubility or enable sensing, targeting, or therapeutic applications. These results position Si-based phthalocyanines as sustainable, high-performance alternatives to precious metal photocatalysts. Looking ahead, the design principles established here offer a foundation for developing next-generation NIR photoinitiators tailored for advanced manufacturing, 3D printing, and light–driven processes in opaque or UV-sensitive environments. More broadly, this study highlights the importance of quantifying photopolymerization efficiency under well-controlled and clearly documented conditions, which will be essential for enabling rigorous comparisons across distinct photochemical systems moving forward.

Author contributions

Conceptualization (C. J. O., Z. A. P.); methodology (C. J. O., L. M. L., T. A. G., J. I., S. T. R., Z. A. P.); investigation (C. J. O., L. M. L., T. A. G., J. I., J. O.); formal analysis (C. J. O., L. M. L., T. A. G., J. I.); visualization (C. J. O., L. M. L., T. A. G., J. I., S. T. R., Z. A. P.); funding acquisition (T. A. G., S. T. R., Z. A. P.); project administration (Z. A. P.); supervision (T. A. G, S. T. R., Z. A. P.); writing – original draft (C. J. O., L. M. L., J. I., Z. A. P.); writing – review & editing (C. J. O., L. M. L., T. A. G., J. I., S. T. R., Z. A. P.).

Conflicts of interest

There are no conflicts to declare.

Data availability

The data supporting this article have been included as part of the SI. See DOI: **https://doi.org/10.1039/d5ta05756f**.

Acknowledgements

The authors acknowledge primary support from the National Science Foundation under grant CHE-2155017 (C. J. O., J. I., S. T. R., Z. A. P). Partial support was provided by the Robert A. Welch Foundation under grant F-2007 (C. J. O., J. I., J. O., Z. A. P); the Center for Electrochemistry at the University of Texas at Austin through the Bard CEC Student Scholar Fellowship under Grant no. H-F-0037 facilitated by the Welch Foundation (C. J. O.); the Research Corporation for Science Advancement under award 28184 (C. J. O., J. O., Z. A. P.); the Finnish Academy of Science and Letters *via* the Foundation's Post Doc Pool grant (J. I.); and the Air Force Research Lab through AFRL/RXEP contract FA8650-22-F-5408 (L. M. L., T. A. G.).

Notes and references

1 R. P. Linstead, *J. Chem. Soc.*, 1934, 1016–1017.
2 A. B. P. Lever, in *Advances in Inorganic Chemistry and Radiochemistry*, Elsevier, 1965, vol. 7, pp. 27–114.
3 N. Kobayashi, S. Nakajima and T. Osa, *Inorg. Chim. Acta*, 1993, **210**, 131–133.
4 D. Wöhrle and D. Meissner, *Adv. Mater.*, 1991, **3**, 129–138.
5 M. R. Singh, C. Xiang and N. S. Lewis, *Sustainable Energy Fuels*, 2017, **1**, 458–466.
6 D. Gounden, N. Nombona and W. E. Van Zyl, *Coord. Chem. Rev.*, 2020, **420**, 213359.
7 R. Zhou, F. Josse, W. Göpel, Z. Z. Öztürk and Ö. Bekaroğlu, *Appl. Organomet. Chem.*, 1996, **10**, 557–577.
8 G. De La Torre, P. Vázquez, F. Agulló-López and T. Torres, *J. Mater. Chem.*, 1998, **8**, 1671–1683.

9 J. F. Van Der Pol, E. Neeleman, J. W. Zwikker, R. J. M. Nolte, W. Drenth, J. Aerts, R. Visser and S. J. Picken, *Liq. Cryst.*, 1989, **6**, 577–592.
10 M. J. Cook, *Chem. Rec.*, 2002, **2**, 225–236.
11 R. Guilard, K. M. Kadish, M. J. Cook, J. Sessler, K. M. Smith and D. Wöhrle, *J. Porphyrins Phthalocyanines*, 2000, 313–318.
12 N. Corrigan, J. Xu and C. Boyer, *Macromolecules*, 2016, **49**, 3274–3285.
13 Z. Wu, K. Jung and C. Boyer, *Angew. Chem., Int. Ed.*, 2020, **59**, 2013–2017.
14 S. E. Korkut, G. Temel, D. K. Balta, N. Arsu and M. K. Şener, *J. Lumin.*, 2013, **136**, 389–394.
15 L. M. Stevens, C. Tagnon and Z. A. Page, *ACS Appl. Mater. Interfaces*, 2022, **14**, 22912–22920.
16 K. Kasuga, T. Miyazako, T. Sugimori and M. Handa, *Synth. React. Inorg. Met.-Org. Chem.*, 2003, **33**, 403–409.
17 K. K. Childress, K. Kim, D. J. Glugla, C. B. Musgrave, C. N. Bowman and J. W. Stansbury, *Macromolecules*, 2019, **52**, 4968–4978.
18 B. D. Rihter, M. E. Kenney, W. E. Ford and M. A. J. Rodgers, *J. Am. Chem. Soc.*, 1993, **115**, 8146–8152.
19 A. Stafford, D. Ahn, E. K. Raulerson, K.-Y. Chung, K. Sun, D. M. Cadena, E. M. Forrister, S. R. Yost, S. T. Roberts and Z. A. Page, *J. Am. Chem. Soc.*, 2020, **142**, 14733–14742.
20 A. Uddin, S. R. Allen, A. K. Rylski, C. J. O'Dea, J. T. Ly, T. A. Grusenmeyer, S. T. Roberts and Z. A. Page, *Angew. Chem., Int. Ed.*, 2023, **62**, e202219140.
21 S. Yamamoto, A. Zhang, M. J. Stillman, N. Kobayashi and M. Kimura, *Chem. - Eur. J.*, 2016, **22**, 18760–18768.
22 N. Kobayashi, S. Nakajima, H. Ogata and T. Fukuda, *Chem. - Eur. J.*, 2004, **10**, 6294–6312.
23 A. V. Soldatova, J. Kim, X. Peng, A. Rosa, G. Ricciardi, M. E. Kenney and M. A. J. Rodgers, *Inorg. Chem.*, 2007, **46**, 2080–2093.
24 A. Cidlina, J. Svec, L. Ludvová, J. Kuneš, P. Zimcik and V. Novakova, *J. Porphyrins Phthalocyanines*, 2016, **20**, 1122–1133.
25 M. Van Leeuwen, A. Beeby, I. Fernandes and S. H. Ashworth, *Photochem. Photobiol. Sci.*, 2013, **13**, 62–69.
26 N. Kobayashi, T. Furuyama and K. Satoh, *J. Am. Chem. Soc.*, 2011, **133**, 19642–19645.
27 T. Furuyama, K. Satoh, T. Kushiya and N. Kobayashi, *J. Am. Chem. Soc.*, 2014, **136**, 765–776.
28 Sigma-Aldrich, Thermal Transitions of Homopolymers: Glass Transition & Melting Point, **https://www.sigmaaldrich.com/US/en/technical-documents/technical-article/materials-science-and-engineering/polymer-synthesis/thermal-transitions-of-homopolymers**.
29 P. A. Firey, W. E. Ford, J. R. Sounik, M. E. Kenney and M. A. J. Rodgers, *J. Am. Chem. Soc.*, 1988, **110**, 7626–7630.
30 M. Wang and K. Ishii, *Coord. Chem. Rev.*, 2022, **468**, 214626.
31 L. Breloy, O. Yavuz, I. Yilmaz, Y. Yagci and D.-L. Versace, *Polym. Chem.*, 2021, **12**, 4291–4316.
32 J. A. S. Cavaleiro, M. J. E. Hewlins, A. H. Jackson and M. G. P. M. S. Neves, *Tetrahedron Lett.*, 1992, **33**, 6871–6874.
33 B. Golec, J. Buczyńska, K. Nawara, A. Gorski and J. Waluk, *Photochem. Photobiol. Sci.*, 2023, **22**, 2725–2734.